ARL-TR-10435 ● SEP 2026

Techniques for Investigations of Nonlinear Optical Effects: Sum-Frequency Generation and Four-Wave Mixing Techniques

by Nhan C. Dang and Frank C. De Lucia Jr.

NOTICES

Disclaimers

ARL-TR-10435 ● SEP 2026

Techniques for Investigations of Nonlinear Optical Effects: Sum-Frequency Generation and Four-Wave Mixing Techniques

Nhan C. Dang and Frank C. De Lucia Jr.
DEVCOM Army Research Laboratory

REPORT DOCUMENTATION PAGE

1. REPORT DATE	2. REPORT TYPE	3. DATES COVERED START DATE	3. DATES COVERED END DATE
September 2026	Technical Report	1 October 2025	30 June 2026

4. TITLE AND SUBTITLE
Techniques for Investigations of Nonlinear Optical Effects: Sum-Frequency Generation and Four-Wave Mixing Techniques

5a. CONTRACT NUMBER	5b. GRANT NUMBER	5c. PROGRAM ELEMENT NUMBER
5d. PROJECT NUMBER	**5e. TASK NUMBER**	**5f. WORK UNIT NUMBER**

6. AUTHOR(S)
Nhan C. Dang and Frank C. De Lucia Jr.

7. PERFORMING ORGANIZATION NAME(S) AND ADDRESS(ES)	8. PERFORMING ORGANIZATION REPORT NUMBER
DEVCOM Army Research Laboratory ATTN: FCDD-RLA-WA Aberdeen Proving Ground, MD 21005	ARL-TR-10435

9. SPONSORING/MONITORING AGENCY NAME(S) AND ADDRESS(ES)	10. SPONSOR/MONITOR'S ACRONYM(S)	11. SPONSOR/MONITOR'S REPORT NUMBER(S)

12. DISTRIBUTION/AVAILABILITY STATEMENT
DISTRIBUTION STATEMENT A. Approved for public release: distribution unlimited.

13. SUPPLEMENTARY NOTES
ORCIDs: Nhan C. Dang, 0009-0000-5752-8330; Frank C. De Lucia Jr., 0000-0003-2759-6978

14. ABSTRACT
Using ultrafast laser techniques, we observe the nonlinear optical responses associated with the upconversion of light in 2D layered materials (2DLM). This report presents our progress in the development of sum-frequency generation and four-wave mixing techniques for measuring the nonlinear optical effects in monolayers of molybdenum disulfide (MoS_2), tungsten disulfide (WS_2), and mono- and bilayers of graphene using near-infrared (NIR) laser pulses. The upconversion of the NIR laser wavelengths due to laser material interactions is reported to demonstrate the experimental capabilities used in the investigation of 2DLMs.

15. SUBJECT TERMS
Weapons Sciences, nonlinear optical properties, optical harmonic generation, 2D layered materials, ultrafast, upconversion

16. SECURITY CLASSIFICATION OF: a. REPORT	b. ABSTRACT	C. THIS PAGE	17. LIMITATION OF ABSTRACT	18. NUMBER OF PAGES
UNCLASSIFIED	UNCLASSIFIED	UNCLASSIFIED	UU	19

19a. NAME OF RESPONSIBLE PERSON	19b. PHONE NUMBER *(Include area code)*
Nhan C. Dang	(520) 691-6422

STANDARD FORM 298 (REV. 5/2020)
Prescribed by ANSI Std. Z39.18

Contents

List of Figures

1. Introduction

The discovery of new materials useful for the next generation of nanophotonic devices such as ultrafast optical frequency switching devices and simplified, compact imaging systems is of interest for applications in the Department of the Army. Two-dimensional layered materials (2DLMs) are attracting attention since 1) they possess nonlinear optical (NLO) properties that can upconvert light frequencies, i.e., they can convert infrared light to visible light and 2) they are chemically and physically stable and possess 2D layered structures, which are suited for nano-film processing. Therefore, 2DLMs have properties that make them desirable candidates for developing highly compact, mobilized, and durable nanophotonic devices.

NLO responses such as second- and third-order nonlinear parametric mechanisms, generated using degenerate photon frequencies, have been observed in a wide variety of 2DLMs.[1–7] The study of nondegenerate parametric processes (i.e., involving two or more photon frequencies), such as sum-frequency generation (SFG) and four-wave mixing (FWM), [8–13] have also been made using 2DLMs. The findings in these studies have shown that 2DLMs have extraordinary NLO properties making them excellent candidates for new types of nanophotonic devices. Using these unique properties, efforts have been made to determine ideal 2DLMs for the development of nanophotonic devices of interest to the U.S. Army. In this work, experimental techniques such as second- and third-harmonic generations (SHG and THG), SFG, and FWM are reported using commercially available layered samples such as monolayers of tungsten disulfide (WS_2), molybdenum disulfide (MoS_2), graphene, and a graphene bilayer.

2. Experimental

2.1 Background

NLO effects are observed in 2DLMs as a response to an interaction with an intense optical field. The NLO process can be described by the induced polarization P in the material and the electric field of the incident light E as follows:

$$P = \varepsilon_0\left(\chi^{(1)}E + \chi^{(2)}E^2 + \chi^{(3)}E^3 \ldots + \chi^{(n)}E^n\right), \qquad (1)$$

where ε_0 is the vacuum permittivity constant and $\chi^{(n)}$ is the nth order NLO susceptibility. The first term, $\chi^{(1)}E$, is related to any linear optical processes, while the rest contribute to the NLO processes. When E is small, the nonlinear part is negligible, resulting in the relation between P and E being linear. However, if incident light is intense, the electric field E becomes more significant, and the contributions of the second and third orders increase—leading to the observation of NLO effects.

The $\chi^{(2)}$ term in Equation 1 describes the second-order NLO susceptibility in a material responsible for second-order NLO processes such as when two wavelengths ($\omega_1$and ω_2) interact with a nonlinear medium to produce a third wavelength (ω_3). When the condition of ω_1= ω_2, this situation is defined as SHG. When $\omega_3 = \omega_1 + \omega_2$ or $\omega_3 = \omega_1 - \omega_2$, they are called SFG and difference-frequency generation (DFG), respectively.

The $\chi^{(3)}$ term in Equation 1 is the third-order NLO susceptibility, which is responsible for third-order NLO processes. FWM is a type of third-order NLO process where three waves (ω_1, ω_2, and ω_3) interact with a nonlinear medium to produce a fourth wave (ω_4). When the condition of ω_1= $\omega_2 = \omega_3$ occurs, i.e., $\omega_4 = 3\omega_1$, THG is obtained. FWM can occur under a variety of wavelength combinations such as $\omega_4 = \omega_1 + \omega_2 + \omega_3$ or $\omega_3 = 2\omega_1 - \omega_2$. The energy level diagrams of SHG, THG, SFG, DFG, and FWM are shown in Figure 1.

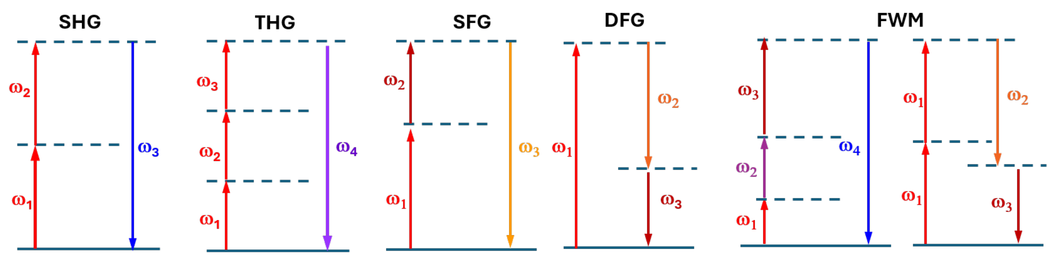

Figure 1. Schematics of SHG, THG, SFG, DFG, and FWM. The full lines represent the real states; the dashed lines represent the virtual states.

2.2 Samples and Sample Configurations

One of the conditions for SHG occurring in these materials is that the sample must be noncentrosymmetric (lack of inversion symmetry). Transition metal dichalcogenides materials (TMDMs) are typically noncentrosymmetric, therefore they exhibit SHG signals intrinsically. On the other hand, materials with centrosymmetric structures, such as graphene and hexagonal boron nitride, have minimal SHG signal. However, at the interface between the centrosymmetric layer and a substrate or another layer, imbalances to the electronic configuration may occur and SHG signals can be produced. This is sometimes referred to as surface SHG. In this report, we selected commercially available 2D monolayers, MoS_2 and WS_2, and mono- and bilayer graphene (2D semiconductors), to test newly developed experimental setups for NLO characterization at the U.S. Army Combat Capabilities Development Command (DEVCOM) Army Research Laboratory

(ARL). The layered samples are grown with chemical vapor deposition and transferred to a quartz substrate. The layers typically have a thickness of 0.6 to 0.8 nm. In Figure 2, we show the sample configuration in relation to the laser pulse input and emission output. Starting from left to right, the pump laser pulse is focused through the 1-mm-thick quartz substrate onto the 2DLMs. Subsequent emission from laser–material interaction continues to the right. The short pass filter then blocks any residual pump laser.

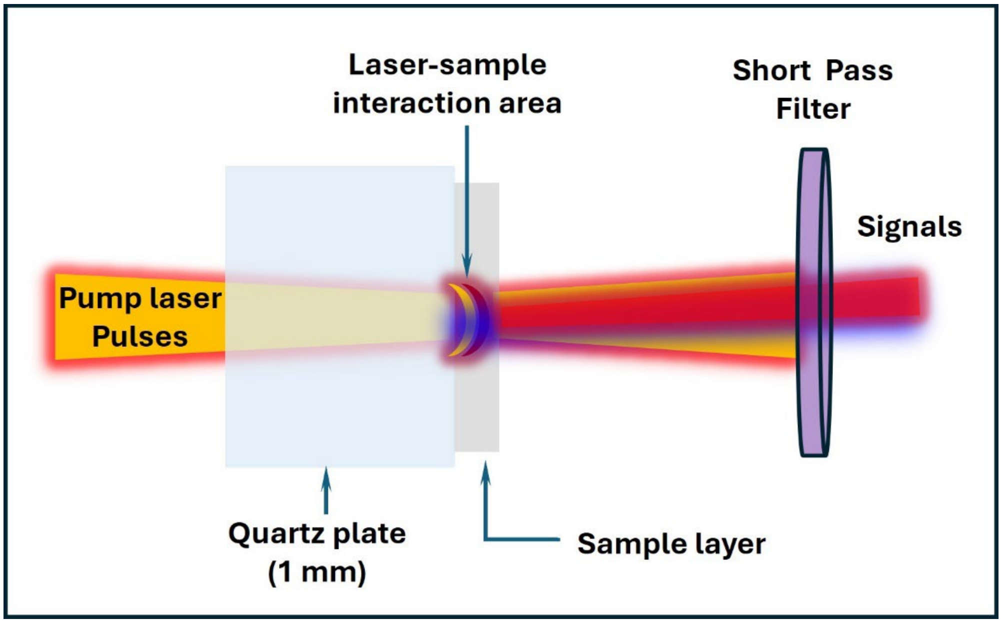

Figure 2. Schematic diagrams of sample configurations used in the SFG and FWM experiments.

2.3 Techniques: Sum-Frequency Generation and Four-Wave Mixing

SFG is a second-order nonlinear process where two incident photons with different frequencies, ω_1 and ω_2, are converted into a photon with a frequency equal to the sum of the two frequencies, $\omega_2 + \omega_1$. To achieve this efficiently, the interacting laser pulses must be phase-matched so that the generated waves constructively interfere as they travel through the medium. FWM is a third-order nondegenerate optical process where three photons can combine in a medium in a variety of combinations generating an output photon or photons. One example of FWM shown in Figure 3 is satisfied by the equation $2\omega_1 - \omega_2 = \omega_3$. Similar to the SFG technique, the interacting laser pulses must be phase-matched to obtain optimal signals of new frequency components. Using a femtosecond laser (Coherent Astrella), we set up two experiments in which both SFG and FWM signals can be simultaneously monitored in the visible wavelength region from 380 to 750 nm by interrogating samples with two laser wavelengths pairs: 777/822 nm and

1198/1300 nm. The experimental setup for the 777- and 822-nm wavelength pair is shown in Figure 3. A single broadband 35-fs, 1-kHz laser pulse centered at 800 nm was first broadened using a four-wave technique.[14] Approximately 2 mJ of the 800-nm laser pulse was directed through a 100-μm-thick beta barium borate (BBO) crystal (Newlight Photonics, BTC10010-SHG800(I)-P) to generate a 400-nm laser pulse. Since the 400-nm pulse was polarized orthogonally to the 800-nm light, a calcite delay compensator (Newlight Photonics, TDC12101-AR-Calcite) was angle-tuned to adjust the delay between the 400-nm pulse and the residual unconverted 800-nm pulse. A dual 800- and 400-nm half-wave plate was used to align the linear polarization of the 400- and 800-nm pulses. These pulses were then focused using a single convex lens with 200-nm focal length to create a high-intensity filament near the focus, where nonlinear self-focusing, self-phase modulation and FWM occur. The spectrum of each of the pulses was broadened through self-phase modulation and mixed with each other to generate FWM signals forming a continuum with new broader bands at 400 and 800 nm compared with the original 400- and 800-nm pump pulses. To spatially separate the new continuum beam from the original 400- and 800-nm residuals, the beam path was directed off center of the single convex lens, and the lens was angled approximately 10° horizontally relative to the beam path. The separated continuum was then collimated by a parabolic mirror. Next, the continuum was spectrally filtered and shaped by a 770-nm long pass filter (Thorlabs, FELH770) and an 800-nm notch filter with a bandwidth of 34 nm (Thorlabs, NF800-34). The resulting spectrum after the filters is shown in Figure 3 (inset) with two collinear laser pulses, peaking at 777 and 822 nm. Temporal overlaps and linear polarizations of these bands were further fine-tuned and aligned using a calcite delay compensator (Newlight Photonics, TDC12101-AR-Calcite) and a 650–1100-nm half-wave plate (Newlight Photonics, WPM03-H-NIR) to get optimal phase-matching. Laser powers of 3 and 12 mW were used at 777 and 822 nm, respectively. The collinear phase-matched pulses were then focused through the back side of the quartz substrate with a 150-mm-focal-length achromatic lens onto the 2DLM sample forming an elliptical focal spot of 250 × 150 μm.

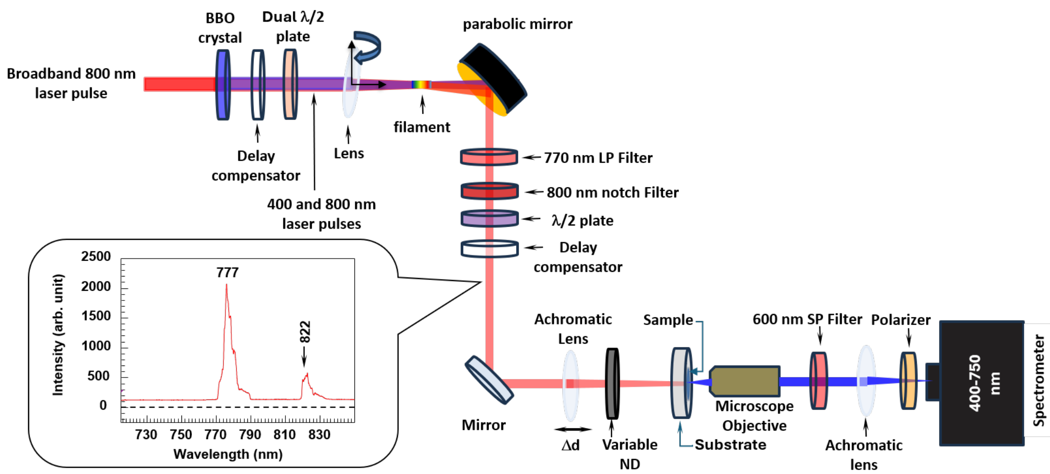

Figure 3. Schematic diagrams of SFG and FWM experimental setup using single pump laser beam with two bands at 777 and 822 nm.

To prevent ablation of sample layers or the formation of a laser-induced plasma in the substrate/sample, the laser energy density was attenuated with a variable neutral density filter and by adjusting the laser beam size on the sample (by adjusting the distance between the sample and the lens) so that the maximum signal was obtained without damage on the sample. Signals generated from the sample were collected using an objective lens (10X Mitutoyo Plan Apo Infinity Corrected Long WD Objective) and refocused with a 75 mm-focal-length achromatic lens through a 600-nm short pass filter (Thorlabs, FESH600) and a linear polarizer (Thorlabs, LPVISSE 100-A) onto a 100-µm slit of a monochromator (Princeton Instruments, 2300i). The residuals of pump laser pulses were filtered out by the 600-nm short pass filter while signal polarization was adjusted with a polarizer. The signal spectrum was dispersed by a monochromator (Princeton Instruments, SpectraPro 2300i) and recorded using an intensified charge-coupled device (ICCD) camera (Princeton Instruments, ICCD Gen-II). The spectral detection window was 380–750 nm. For the pump laser pulses 777 and 822 nm, the expected signals are SHGs at 389 nm ($2\omega_1$) and 411 nm ($2\omega_2$), SFG at 399 nm ($\omega_1 + \omega_2$), and FWM at 737 nm ($2\omega_2 - \omega_1$).

Figure 4 depicts the experimental setup for the 1198- and 1300-nm wavelength pair. To generate these two pulses, an optical parametric amplifier (OPA) (Coherent, Opera Solo) coupled with a 35-fs, 1-kHz laser pulse centered at 800 nm (Coherent, Astrella) was used. To generate 1198- and 1300-nm laser pulses, the output of the OPA was at 1275 nm. A 1200-nm short pass dichroic mirror (DM) (Thorlabs, DMSP1200R) was used to split the broadband output into two beams, where the beam with the wavelengths shorter than 1200 nm passed through the DM while the beam with wavelengths longer than 1200 nm were reflected by the DM. To generate narrow bands of 1198- and 1300-nm pulses, the beam with shorter wavelengths than 1200 nm was spectrally filtered by a 1200-nm band pass filter with a band width of 12 nm (Thorlabs, FBH1200-12), while the reflected beam with longer wavelengths than 1200 nm passed through a 1300-nm band pass filter with a band width of 12 nm (Thorlabs, FBH1300-12). These two narrow-band laser pulses were then recombined and spatially and temporally overlapped at the second 1200-nm short pass DM (Thorlabs, DMSP1200R), where the 1198-nm pulse passed through the second DM and was colinearly aligned with the 1300-nm pulse that was reflected by the other surface of the second DM. The resulting spectrum of these two pulses is shown in Figure 4 (inset). The 1198- and 1300-nm pulses were then fine-tuned for optimal phase-matching using a delay compensator (Newlight Photonics, THG800-A10-35fs) and a dual wavelength half-wave plate (Newlight Photonics, WPM04-H-775-1550). The pulses were focused on the sample using an achromatic lens forming an elliptical focal spot size of 250 × 150 µm. Laser powers of 2.5 and 12.5 mW were used at 1198- and 1300-nm, respectively. The total energy density on the 2DLM from the pulses is controlled by a variable neutral density filter and the distance between the lens and the 2DLM. NLO signals were collected with a microscope objective (same as above). An 800-nm short pass filter (Thorlabs, FESH800) is used to cut out the residuals of the 1198- and 1300-nm pump laser pulses and then the NLO signals were focused into the spectrometer described previously. The expected signals are SHGs at 599 ($2\omega_1$) and 650 nm ($2\omega_2$), THGs at 399 ($3\omega_1$) and 433 nm ($3\omega_2$) due to 1198- and 1300-nm pump pulses, respectively; SFG at 623 nm ($\omega_1 + \omega_2$); and FWM at 410 ($2\omega_2 + \omega_1$) and 421 nm ($2\omega_1 + \omega_2$).

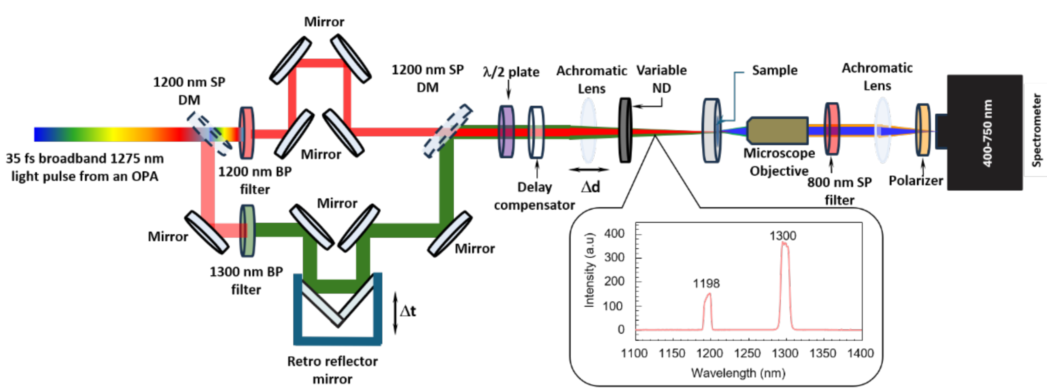

Figure 4. Schematic diagrams of SFG and FWM experimental setup using pump laser wavelengths of 1198 and 1300 nm.

We generated all reported spectra by accumulating 500 spectra using a 1-s collection window for each spectrum and then subtracting with the spectrum of a blank quartz substrate recorded under identical experimental conditions.

3. Results and Discussions

3.1 SHGs, SFG, and FWM Using 777- and 822-nm Pump Laser Wavelengths

Figures 5 and 6 depict NLO effects that occur in WS_2 and MoS_2 monolayers, respectively, when illuminating the sample with 777- and 822-nm laser pulses. The reported spectra here are of the NLO responses at three different locations on the surface of the sample. As expected, strong SFGs at 399 nm are observed, while weak FWM signals (insets) appear at 737 nm in both samples. In addition to the SFG and FWM signals, strong SHGs show at 389 and 411 nm due to interaction of the samples with the 777- and 822-nm single pulses, respectively. The SFG and SHG signal intensities generated in these two samples are different at different locations on the sample surface. These observations indicate that the 2DLM samples are not completely homogeneous across the substrate surfaces.

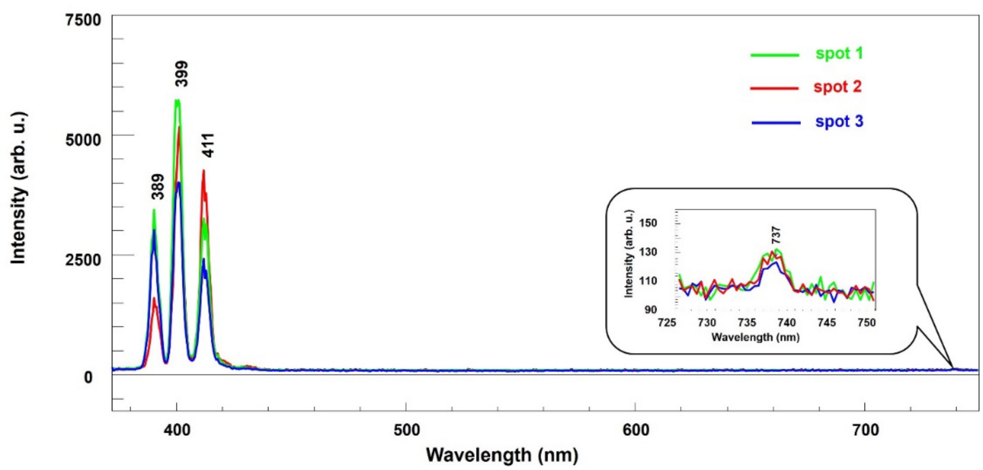

Figure 5. SHGs, SFG, and FWM signals generated by interacting 777- and 822-nm laser pulses with WS_2.

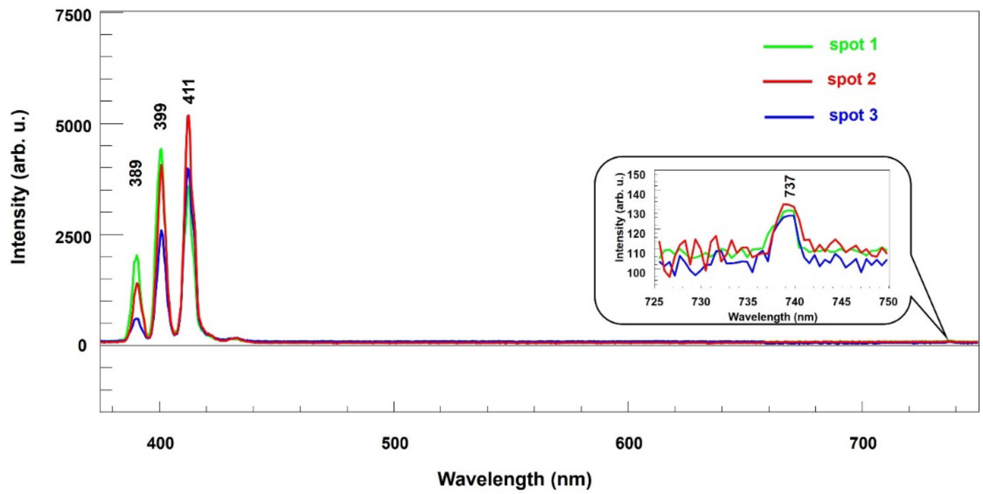

Figure 6. SHGs, SFG, and FWM signals generated by interacting 777- and 822-nm laser pulses with MoS_2.

3.2 SHGs, THGs, SFG, and FWMs Using 1198- and 1300-nm Pump Laser Wavelengths

Figures 7 and 8 depict NLO effects that occur at three different spots in WS_2 and MoS_2 monolayers, respectively, when illuminating the sample with 1198- and 1300-nm laser pulses. Strong second-order processes are observed compared with third-order processes. Two strong peaks of SHGs and one strong peak of SFG (generated due to interaction of the samples with the 1198 and 1300 nm) are observed at 599, 650, and 623 nm, respectively. FWM signals were observed at 410 and 421 nm. THGs (generated due to interaction of the samples with the individual 1198 and 1300 nm) were observed at 399 and 433 nm.

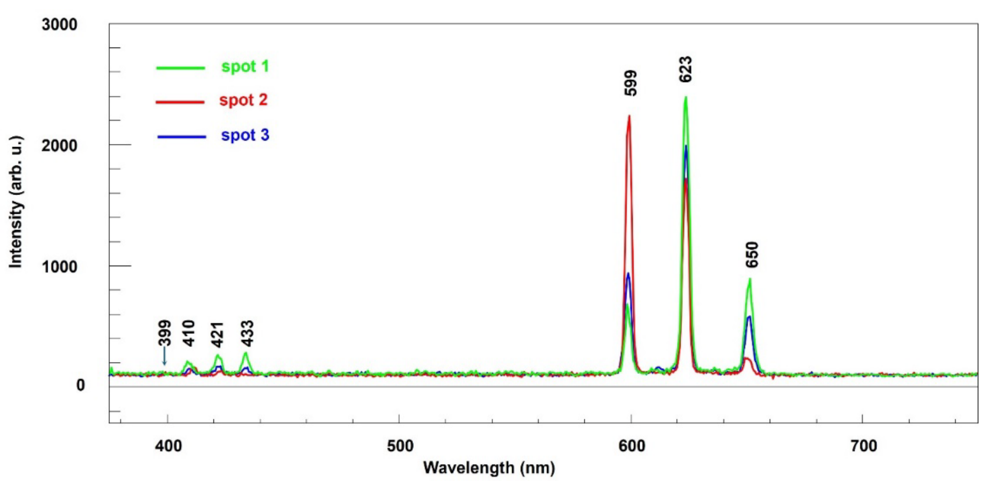

Figure 7. SHGs, THGS, SFG, and FWM signals generated by interacting 1198- and 1300-nm laser pulses with WS_2.

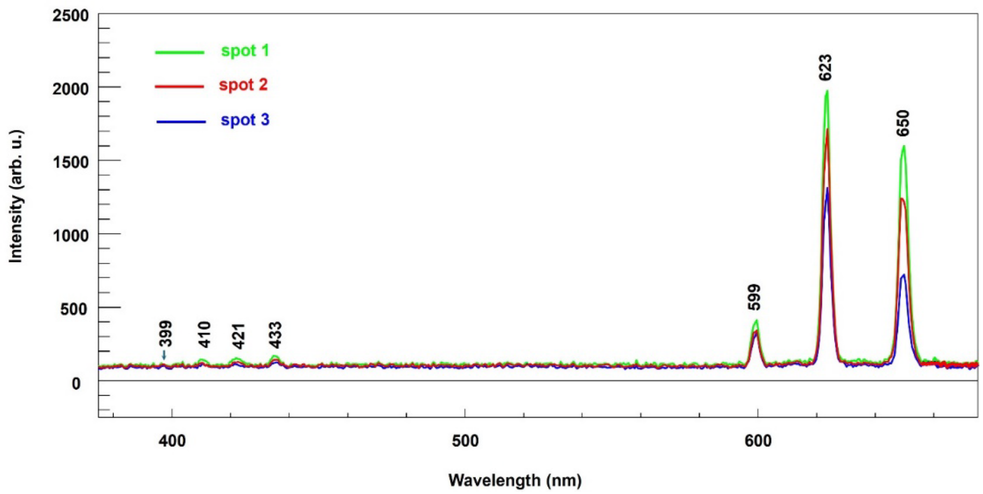

Figure 8. SHGs, THGS, SFG, and FWM signals generated by interacting 1198- and 1300-nm laser pulses with MoS_2.

To investigate NLO effects in 2DLMs with centrosymmetric structures that are modified to have imbalance in electronic configurations, a graphene monolayer and stacked graphene bilayer samples were chosen. Figure 9 shows NLO effects occurring in these samples. In this figure, as expected, no SHG or SFG is observed for the centrosymmetric graphene monolayer (green curve). However, for the graphene bilayer, due to stacking of the two monolayers in which the monolayers are bonded by Van der Waals forces, the sample becomes noncentrosymmetric (i.e., imbalance in electronic configurations), therefore SHG and SFG is observed. Like WS_2 and MoS_2, the graphene bilayer sample, when interacting with the 1198- and 1300-nm laser pulses, gives a strong SFG peak at 623 nm, and SHG peaks at 599 and 650 nm. No FWM or THG signals are observed in the graphene bilayer.

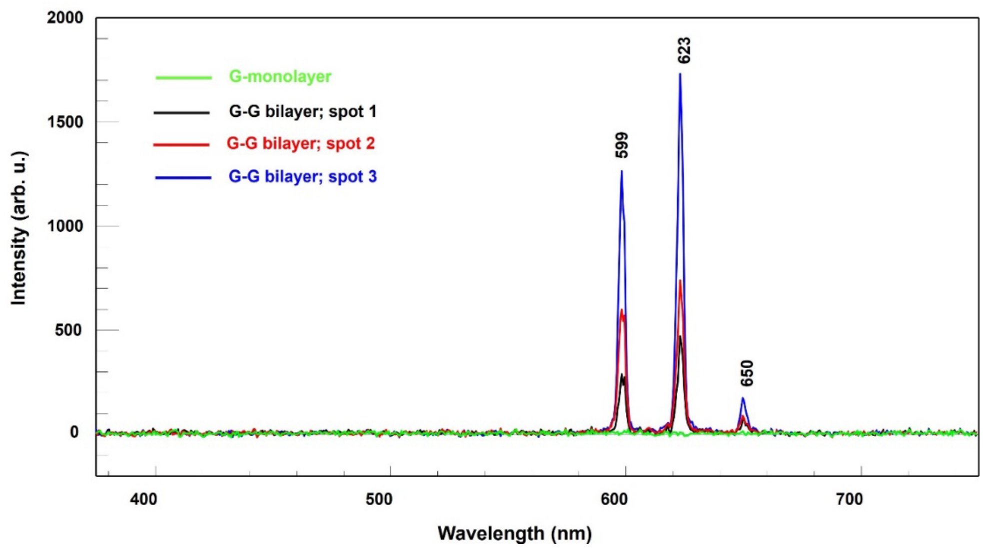

Figure 9. SHGs, THGS, and SFG signals generated by interacting 1198- and 1300-nm laser pulses with graphene (G) mono- and bilayers.

4. Conclusion

Using our ultrafast experimental capabilities, we are developing essential tools for investigating the NLO effects in 2DLMs—materials that are the key for creating next-generation nanophotonics due to their diverse characteristics. The ability to measure NLO effects can be used to characterize 2DLM properties such as number of layers, defects in the layer, orientation angles, and mechanical strain, to name a few. Furthermore, the NLO response can be used to optimize the performance of potential new 2DLM-based devices.

5. References

1. Säynätjoki A et al. Ultra-strong nonlinear optical processes and trigonal warping in MoS_2 layers. Nat Commun. 2017;8:1−8.
2. Le CT et al. Nonlinear optical characteristics of monolayer $MoSe_2$. Ann Phys. 2016;528:551−559.
3. Autere JH et al. Optical harmonic generation in monolayer group-VI transition metal dichalcogenides. Phys Rev B Condens Matter Mater Phys. 2018;98:115426.
4. Beams R et al. Characterization of few-layer 1T $MoTe_2$ by polarization-resolved second harmonic generation and Raman scattering. ACS Nano. 2016;10:9626−9636.
5. Ribeiro-Soares J et al. Second harmonic generation in WSe_2. 2D Mater. 2015;2:045015.
6. Janisch C et al. Ultrashort optical pulse characterization using WS_2 monolayers. Opt Lett. 2014;39:383−385.
7. Janisch C et al. Extraordinary second harmonic generation in tungsten disulfide monolayers. Sci Rep. 2015;4:5530.
8. Li D et al. Multimodal nonlinear optical imaging of MoS_2 and MoS_2-based van der Waals heterostructures. ACS Nano. 2016;10:3766−3775.
9. Jakubczyk T et al. Radiatively limited dephasing and exciton dynamics in $MoSe_2$ monolayers revealed with four-wave mixing microscopy. Nano Lett. 2016;16:5333−5339.
10. Bolhuis M et al. Vertically-oriented MoS_2 nanosheets for nonlinear optical devices. Nanoscale. 2020;12:10491−10497.
11. Dai Y et al. Electrical control of interband resonant nonlinear optics in monolayer MoS_2. ACS Nano. 2020;14:8442−8448.
12. Hao K et al. Direct measurement of exciton valley coherence in monolayer WSe_2. Nat Phys. 2016;12:677−682.
13. Jakubczyk T et al. Impact of environment on dynamics of exciton complexes in a WS_2 monolayer. 2D Mater. 2018;5:031007.
14. Fuji T, Suzuki T. Generation of sub-two-cycle mid-infrared pulses by four-wave mixing through filamentation in air. Opt Lett. 2007;32(22):3330–3332.

List of Symbols, Abbreviations, and Acronyms

2D	Two-Dimensional
2DLM	Two-Dimensional Layered Materials
ARL	Army Research Laboratory
BBO	Beta Barium Borate
DEVCOM	U.S. Army Combat Capabilities Development Command
DFG	Difference-Frequency Generation
DM	Dichroic Mirror
FWM	Four-Wave Mixing
ICCD	Intensified Charge-Coupled Device
MoS_2	Molybdenum Disulfide
NIR	Near Infrared
NLO	Nonlinear Optical
OPA	Optical Parametric Amplifier
SFG	Sum-Frequency Generation
SHG	Second-Harmonic Generation
THG	Third-Harmonic Generation
TMDM	Transition Metal Dichalcogenides Materials
WS_2	Tungsten Disulfide

1 (PDF)	DEFENSE TECHNICAL INFORMATION CTR DTIC OCA
1 (PDF)	DEVCOM ARL FCDD RLB CB TECH LIB